

Electrokinetic characterization of extracellular vesicles with capillary electrophoresis: a new tool for their identification and quantification

Marco Morani¹, Thanh Duc Mai¹, Zuzana Krupova², Pierre Defrenai², Evgen Multia³, Marja-Liisa Riekkola³ and Myriam Taverna^{1,4*}

¹ *Institut Galien Paris Sud, UMR 8612, Protein and Nanotechnology in Analytical Science (PNAS), CNRS, Univ. Paris-Sud, Univ. Paris-Saclay, 5 rue Jean Baptiste Clément, 92290 Châtenay-Malabry, France*

² *Excilone - 6, Rue Blaise Pascal - Parc Euclide - 78990 Elancourt - France*

³ *Department of Chemistry, P.O. Box 55, FI-00014 University of Helsinki, Finland.*

⁴ *Institut Universitaire de France (IUF)*

Correspondence: E-mail: myriam.taverna@u-psud.fr; Fax: +33-1-46-83-54-62

Keywords: capillary electrophoresis; LIF detection; membrane labeling; extracellular vesicles

Abbreviations: EVs, extracellular vesicles; CE, capillary electrophoresis; LIF, laser-induced fluorescence; DLS, dynamic light scattering; NTA, nanoparticle tracking analysis; PVA, polyvinyl alcohol; AsFIFFF, Asymmetrical flow field-flow fractionation; MALS, multi angle light scattering; ISF BGE, inorganic-species-free background electrolyte; SEC, size exclusion chromatography.

Abstract

This work reports on the development of the first capillary electrophoresis methodology for the elucidation of extracellular vesicles' (EVs) electrokinetic distributions. The approach is based on capillary electrophoresis coupled with laser-induced fluorescent (LIF) detection for the identification and quantification of EVs after their isolation. Sensitive detection of these nanometric entities was possible thanks to an 'inorganic-species-free' background electrolyte. This electrolyte was made up of weakly charged molecules at very high concentrations to stabilize EVs, and an intra-membrane labelling approach was used to prevent EV morphology modification. The limit of detection for EVs achieved using the developed CE-LIF method reached 8×10^9 EVs / mL, whereas the calibration curve was acquired from 1.22×10^{10} to 1.20×10^{11} EVs / mL. The CE-LIF approach was applied to provide the electrokinetic distributions of various EVs of animal and human origins, and visualize different EV subpopulations from our recently developed high-yield EV isolation method.

1. Introduction

Extracellular vesicles (EVs) are a common family of heterogeneous small vesicles secreted by all types of cells. [1, 2]. EVs contain distinct subsets of molecules characteristic of the mother cells from which they are secreted, conveying, in this way, many vital signals under normal or pathological conditions. This makes them useful for biomarker discovery and much current research is focusing on them for their potential diagnostic and prognostic applications [3-5]. Despite overt evidence of the potential of EVs in clinical diagnostic practice, guidelines for analytical procedures have not yet been properly established. The isolation and enrichment of EVs from biofluids remains a challenging prerequisite before light can be shed on the target exosomal molecules (e.g. nucleic acids, proteins, growth factors, cytokines etc.) that are present in trace amounts. After this has been achieved, it is critical to verify the identity of EVs and monitor their purity and concentration.

Until now, most common physical characterization approaches have relied on microscopy-based methods, dynamic light scattering (DLS), nanoparticle tracking analysis (NTA) and tunable resistive pulse sensing vesicle flow cytometry (see [6, 7]). To a lesser extent, immunoaffinity-based methods, notably enzyme-linked immunosorbent assays (ELISA) and amplified luminescent proximity homogeneous assay on beads (ExoScreen), have been employed to identify EVs' subpopulations from different cellular origins [8, 9]. Each technique can provide only part of the information sets required for the confirmation and characterization of target EVs. EVs identification can also be done via analyses of exosomal lysates (e.g. immunoblotting or mass spectrometry for intra-exosomal proteins [6], or Fluorocet kit to measure esterase activity released from lysed EVs [10]). Nevertheless, with such bulk measurements, the differentiation between small cells, debris and EVs may not be possible, and information on size and charge is not provided. To have access to reliable and fast identification and characterization of EVs, continued efforts have been directed toward the development of

novel technologies. The most recent communications reported on exosome luminescent quantification [11] and electrical detection of polarized exosomes via capacitance-voltage measurements [12].

A satisfactory method should meet all the criteria for EV phenotyping, notably the ability to discriminate between different size sub-populations and to maintain EV integrity during analysis. High detection sensitivity in some cases is desirable, for example when working with EVs from cerebrospinal fluids, as their concentration after extraction may be very low. Till now, no single method has succeeded in meeting all of these criteria simultaneously or that can be used universally in a variety of infrastructures (i.e. depending on the equipment and expertise to hand). To provide sufficient physical and biological information on isolated EVs many complementary techniques have to be used. From this rationality, capillary electrophoresis (CE), which has shown its capability to provide nanoparticle analysis and characterization [13], emerges as an interesting and unexplored alternative to elucidate the electrokinetic distribution of nanoscaled EVs. The only electrokinetic approach, based on electrophoretic light scattering, was exploited by Ichiki's group for tracking exosomes and measuring their zeta potential, using a microchip format coupled with a laser dark-field microscope [14-16]. In addition, specific purpose-made instrumentation and manual operation are required for this new application.

Herein we report for the first time the use of CE coupled with laser-induced fluorescent (LIF) detection for the identification and quantification of EVs after their isolation. To this purpose, strategies for fluorescent labeling of EVs, EVs matrix substitution as well as background electrolyte optimization were developed. Then the developed CE-LIF method was employed to study the electrokinetic distribution of EVs isolates obtained from using various techniques, including the recently developed approach for high-yield EV isolation from human plasma [17].

After the submission of our manuscript on CE-LIF of EVs, another work on CE-UV of EVs was published [18]. Together with this pioneering work, we provide herein the first proof of concept on electrokinetic separation and characterization of EVs.

2. Materials and methods

2.1. Chemicals and reagents

2-(Cyclohexylamino)ethanesulfonic acid (CHES), phosphate buffered saline (PBS 10x), sodium dodecyl sulfate (SDS, 98.5% (GC)), Tris(hydroxymethyl)aminomethane (Tris) and sodium acetate, anhydrous Na₂CO₃, NaHCO₃, and phosphate buffer saline tablets (PBS) were all obtained from Sigma Aldrich (St. Louis, MO, USA). Sodium hydroxide (1 M), hydrochloric (1 M) and acetic (99.9% purity) acids were obtained from VWR (Fontenay-sous-Bois, France). All buffers were prepared with deionized water. Vybrant™ CFDA SE Cell Tracer Kit (dye 5-(and-6)-Carboxyfluorescein diacetate succinimidyl ester, CFDA-SE) was purchased from Thermo Fisher Scientific (Waltham, MA, USA). 25% (v/v) ammonia was obtained from Riedel-de Haën (Seelze, Germany). CD9 Monoclonal Antibody (eBioSN4 (SN4 C3-3A2)), eBioscience™ was purchased from Thermo Fisher Scientific and purified mouse anti-human CD61 (clone VI-PL2) antibody was purchased from BD Biosciences (San Jose, CA, USA). CIM® CDI -0.34 mL disks and the disk housing were purchased from BIA Separations (Ajdovščina, Slovenia). Healthy human plasma for immunoaffinity isolations of EVs was obtained from Finnish Red Cross Blood Service (Helsinki, Finland). EVs samples of different purity degrees isolated from bovine milk, pony plasma, pony serum, and human plasma were provided by Excilone (Elancourt, France).

2.2. Apparatus and Material

The CE-LIF studies were performed with a PA 800 Plus system (Sciex Separation, Brea, CA) equipped with a solid-state laser induced fluorescence detector ($\lambda_{\text{excitation}}$: 488 nm, $\lambda_{\text{emission}}$: 520 nm) purchased from Integrated Optics (Art. No. 40A-48A-52A-64A-14-DM-PT, distributed by Acal BFi, Evry, France). Uncoated fused silica capillaries were purchased from CM Scientific (Silsden, UK). Polyvinyl Alcohol (PVA) neutral capillaries were obtained from Sciex. Data acquisition and instrument control were carried out using Karat 8.0 software (Sciex Separation, Brea, CA). Deionized water used in all experiments was purified using a Direct-Q3 UV purification system (Millipore, Milford, MA, USA). Conductivity and pH values of buffer solutions and samples were obtained with a SevenCompact pH meter (Mettler Toledo, Schwerzenbach, Switzerland). Preparation of background electrolyte (BGE) and buffer ionic strength (IS) calculations were based on simulations with the computer program Phoebus (Analis, Suarlée, Belgium).

Asymmetrical flow field-flow fractionation (AsFIFFF) system used was from Postnova Analytics (AF2000 system, Landsberg, Germany). It was equipped with 350 μm spacer (Postnova Af2000 MF) and a 10 kDa mass cut-off regenerated cellulose membrane (Postnova AF2000 MT series) in a kite shaped channel ($L_{\text{tot}}=27.5$ cm). The channel was followed by UV (SPD-20A Prominence, Shimadzu, Japan), multi-angle light scattering (MALS) (BI-MwA Molecular Weight Analyzer, USA), and DLS (Zetasizer Nano, Malvern Instruments, UK) detectors. The fractions were collected with CBM-20A modular system controller (Shimadzu, Japan) and FRC-10A fraction collector (Shimadzu, Japan). Fractions were further lyophilized for EVs enrichment using Heto PowerDry LL1500 freeze dryer (Thermo Scientific).

2.3. Methods

Isolation of bovine milk-derived EVs with sucrose gradient ultracentrifugation

Whole bovine milk samples were centrifuged at 3,000 x g for 30 min at 4°C (Allegra X-15R, Beckman Coulter, France) to separate fat from skimmed milk. The whey was obtained after acid precipitation of milk (50 mL) with 5 mL of 10% acetic acid and incubation at 37 °C for 10 minutes. This was then continued by addition of 5 mL of 1 M sodium acetate, and incubation for 10 minutes at RT. This was followed by centrifugation at 1500 x g, 4°C for 15 min and filtration of supernatant using vacuum-driven filtration system Millipore Steritop, 0.22 µm. The whey supernatants were concentrated by centrifugation at 4,000 x g and 20°C using Amicon 100kDa centrifugal filter units (Merck Millipore). The obtained retentate was ultra-centrifuged for pelleting the EVs at 100 000 x g for 1h10 at 4°C (Beckman Coulter, Optima XPN-80, 50TI rotor). The pellets were solubilized in 500 µL of PBS then added to 11 mL of pre-prepared sucrose gradient 5-40% and ultra-centrifuged at 200 000 x g for 18h at 4°C (Beckman Coulter, Optima XPN-80, SW41 rotor). Selected fractions corresponding to EVs' flotation densities (1 mL) were collected, diluted in 6 mL of PBS 1x and finally centrifuged at 100 000 x g for 1h10 at 4°C (Beckman Coulter, Optima XPN-80, 50TI rotor). The pellets were resuspended in 50 µL of PBS 1x and stored at -80°C, until further analyses. Bovine milk-derived EVs with narrow size distribution, well-determined concentrations and characterized with dynamic light scattering (DLS), nanoparticle tracking analysis (NTA), transmission electron microscopy (TEM) as well as proteomic profiling were used as EV standards for CE-LIF methodology development.

Isolation of pony plasma/serum and human plasma derived EVs with size exclusion chromatography (SEC)

Preparation of plasma: Peripheral blood was collected into EDTA-coated vacutainer tubes. After ten-time inversion, samples were processed within the 60 minutes of collection. Consecutive centrifugation steps at 2,500 x g, 4°C for 15 minutes and then at 15 000 x g for 10

minutes were performed followed by filtration of the supernatant through 0.22µm filters.

Preparation of serum: Whole blood was collected into anticoagulant-free tubes and allowed to clot at room temperature for 45 minutes. The clot was removed by centrifuging at 3 200 x g, 4°C for 15 minutes, followed by centrifugation at 15 000 x g, 4°C for 10 minutes and filtration of the supernatant through 0.22 µm filters.

500 µl of pre-treated plasma/serum was loaded onto a qEVoriginal SEC column (Izon Science, New Zealand) previously washed and equilibrated with PBS. Fraction collection (0.5 mL per fraction) was carried out immediately using PBS as elution buffer. The selected elution fractions were pooled and were subsequently concentrated using 100 kDa Amicon centrifugal filter units (Merck Millipore). Post-treatment processing with several washing steps with PBS was applied to obtain highly pure EV fractions.

Isolation of human plasma derived EVs with monolithic disks via immunoaffinity chromatography

EVs were isolated from human plasma using a recently developed monolithic affinity chromatography approach [17]. Briefly, diluted human plasma samples (250 µL of plasma diluted to 5 mL in PBS) were percolated through monolithic disk columns immobilised with either anti-human CD61 or anti-human CD9 antibodies. The enriched EVs were eluted with 2 mL of either ammonium hydroxide (NH₄OH, pH 11.3) or carbonate-bicarbonate (pH 11.3) solution after washing the unbound plasma with 3 mL of PBS. The ammonium hydroxide solution was prepared by diluting 2.26 mL of 25% ammonia to a final volume of 100 mL with Milli-Q water. The carbonate-bicarbonate solution was prepared by mixing 90 mL of 0.1 M Na₂CO₃ stock solution (1.06 g of anhydrous Na₂CO₃ dissolved in 100 mL of Milli-Q water) with 10 mL of 0.1 M NaHCO₃ stock solution (0.84 g of NaHCO₃ in 100 mL of Milli-Q water) and adjusting the pH to 11.3 with 200 µL of 5 M NaOH. The pH of the isolates (final volume

0.5 mL) was adjusted by addition of 50 μ L of 1 M HCl prior to characterization with Lowry method [19], NTA, Western blotting, and TEM [20]. The results of these characterizations can be found in our previous study [17].

Asymmetrical flow field-flow fractionation (AsFIFFF) coupled with UV, multi-angle light scattering (MALS) and flow DLS detectors were used to characterize and fractionate subpopulations of the eluents. EV isolation and characterization were performed using the protocol recently published [17] with some modifications. Briefly, 500 μ L was injected with a flow of 0.1 mL/min over 5 min during the focus mode at the cross-flow rate of 3 mL/min. Detector flow rate was 0.5 mL/min and PBS was used as a running buffer. After the focusing step and 1 min of transition time, a 2 min linear decrease in cross-flow to 0.5 mL/min was implemented, followed by a linear decrease over 1 min to 0 mL/min. The run was continued for 15 min with only the detector flow (0.5 mL/min), followed by a rinse step (0.5 mL/min) for 2 min, making a total run time of 26 min. EV fractions (300 μ L each) provided by AsFIFFF were frozen and subsequently lyophilized over 3 hours at temperature of -110°C . Before starting the labelling protocol, the fractions were rehydrated with 30 μ L PBS for EVs enrichment.

Dynamic Light Scattering (DLS) of extracellular vesicles

Size distribution and zeta potential of EVs were measured using a Zetasizer Nano (Malvern Instruments, Malvern, UK). All measurements, using PBS as the dispersant, were undertaken in triplicates at 25°C with scattering angle of 90° and refractive index of 1.332. Data processing and analysis were performed in the automatic mode with at least 13 measurements per run using Zetasizer software version 7.11.

Nanoparticle Tracking Analysis (NTA) of extracellular vesicles

Size distribution and particle concentration were determined with either Nanoparticle Tracking Analysis (NTA) systems: Zetaview (Particle Metrix, Germany) or Nanosight (Malvern Instruments, UK). All experiments were carried out with pre-diluted samples in PBS according to input sample concentrations, leading to particle concentration within the 10^7 - 10^9 particles per mL range for optimal analysis.

The Zetaview system (Particle Metrix) was equipped with a 488 nm laser. Each experiment was performed in duplicate on 11 different positions within the sample cell with following specifications and analysis parameters: sensitivity 60, shutter 100, Max Area 100, Min Area 5, Min Brightness 25. The results were validated while obtaining at least 1 000 valid tracks for each run. For data capture and analysis, the Nanoparticle Tracking Analysis Software (NTA) vs 8.05.04 was used.

Particle concentration and size distribution were also determined with a Nanosight NS300 instrument (Malvern, version NTA 3.2 Dev Build 3.2.16) equipped with a 405 nm laser, sCMOS camera type and the NTA software v3.1. The video acquisition was performed using a camera level of 14. Per sample, 3 videos of 90 seconds with a frame rate of 30 frames/s were captured at 25°C and subsequently analyzed with a threshold set up at 5. The results were validated with at least 2,000 valid tracks for each triplicate.

Fluorescent labelling of EVs

The fluorescently labelled EVs were prepared using the 5-(and-6)-Carboxyfluorescein diacetate succinimidyl ester (CFDA-SE). The CFDA-SE stock solution (10 mM) was prepared in DMSO following the manufacturer's instructions. Prior to staining, the working solution was diluted to 200 μ M in PBS. 20 μ L of EVs was mixed with 20 μ L of 200 μ M CFDA-SE solution (resulting in a final CFDA-SE concentration of 100 μ M), and incubated for 2h in the dark at 37°C with gentle shaking.

Matrix substitution of EVs

Labelled EVs were obtained from two different matrix exchange approaches, using either centrifugal filtration on Nanosep Omega Membranes 3K (PALL Life Sciences, Port Washington, NY, USA) or EVs filtration with commercial Exosome Spin Columns (MW 3000) obtained from Thermo Fisher Scientific (Waltham, MA USA). The first approach (centrifugal filtration) was carried out by addition of the desired buffer to be substituted on the top of the labelled EVs, then centrifugal spinning of the column for approximately 4 minutes at 5000 x g. This process was repeated four times. In the last step, a buffer volume equivalent to that of labelled EVs was used to maintain the same concentration before and after filtration. The second approach was carried out according to the manufacturer's instructions.

CE-LIF of fluorescently labelled EVs and EOF measurement

The fused silica capillary (I.D. of 50 μm , O.D. of 375 μm effective length (L_{eff}) of 50.2 cm and total length (L_{tot}) of 60.2 cm) was pre-conditioned (using a pressure of 172 kPa at the capillary inlet) with the following sequence: water for 10 min, 1 M NaOH for 10 min, 1 M HCl for 10 min and then water for 10 min. The rinsing between two analyses was carried out with 50 mM SDS for 5 min, 1 M NaOH for 5 min, deionized water for 5 min, and finally the running BGE for 5 min using a pressure of 207 kPa. A plug of sample was hydrodynamically injected from the inlet end by applying a pressure of 3.4 kPa for 2 min. The separation was carried out under 25 kV (normal polarity) at 25 °C and the samples were maintained at 5 °C with the sample storage module of the PA 800 Plus equipment. The optimized BGE was composed of Tris / CHES (IS 90 mM, pH 8.4). This BGE was prepared as follows. First two stock solutions of 1.5 M Tris and 1.2M CHES were prepared by dissolving 1.817 g of Tris base in 10 mL of water and 10.447 g of CHES in 42 mL of water. Then, 8 mL of 1.5 M Tris was mixed with 41.09 mL

of 1.2 M CHES. Deionized water was then added to a total volume of 50 mL. pH of the BGE after preparation was confirmed with a pH meter.

The calibration curve was acquired using bovine milk derived EV standards. The EVs isolates were diluted with 1X PBS to prepare different initial EVs concentrations from 1.65×10^{10} to 1.65×10^{11} EVs / mL before the labeling and matrix removal on spin columns. 20 μ L of EVs was mixed with 20 μ L of CFDA-SE 200 μ M solution (resulting in a final CFDA-SE concentration of 100 μ M CFDA-SE), and incubated for 2 h at 37°C. Then 40 μ L of labelled EVs was loaded into EV Spin Columns and recovered in Tris / CHES 90 mM. Calculations for final concentrations were based on initial concentration measured by NTA before the labeling and taking into account a recovery of 75 % from the matrix substitution step. EO mobility was measured with CE-LIF using 4-(4-Methoxybenzylamino)-7-nitro-2,1,3-benzoxadiazole (MBD, used as an EOF marker) which is a neutral and fluorescent compound [21]. The EOF marker was dissolved in a DMSO:CH₃OH (1:1 v/v) solution to a concentration of 20mM, and then further diluted to 2 mM in BGE before use.

3. Results and Discussion

3.1. Fluorescent labeling of EVs

Our preliminary attempts to determine EVs with CE-UV showed insufficient sensitivity in detecting low-abundant milk EVs purified by ultracentrifugation and suspended in PBS. To improve the detection sensitivity and specificity, an effort was made to specifically tag EVs with a fluorescent dye for CE-LIF analysis. Among the different available strategies for the fluorescent labelling of EVs [22-25], the intra-membrane labelling approach using CFDA-SE, initially applied for flow cytometry of EVs derived from dendritic cell lines, was reported to result in no changes in size or charge of EVs [25]. This approach also avoided previous issues encountered with lipophilic dyes that form dye aggregates or micelles with similar signals to

those of EVs, thereby inducing misleading data [26]. This intracellular covalent protein tagging method was therefore adapted to CE-LIF with further optimisations to label EVs. Different parameters, including incubation temperature, duration, dye concentration as well as agitation mode and speed, were optimized to achieve the highest difference between LIF signals of milk EVs samples and those from blanks (see Fig. S1 in the Electronic Supplementary Information ESI). We observed that EVs staining reached the saturation at dye concentrations higher than 200 μ M (Fig. S1 A). By varying the EVs dye incubation time from 30 min to 12 hours, it was found that much longer incubation times (at least 2 hours) were required for EVs labelling than those normally used for cell labelling with CFDA-SE (5-15 min) [27]. This is presumably due to differences in size and esterase expression. Too long incubation time on the other hand resulted in lower signal-to-noise ratio in a time-dependent manner (Fig. S1 B), possibly due to EVs lysis or breaking of the covalent linkage in fluorescent dye over long time. Optimal conditions for EVs labelling with CFDA-SE were set at 37 °C, 2 hours of incubation, and shaking at 300 rpm. Quality control of CFDA-SE labelled EVs using DLS and NTA (see Fig. S2) revealed no significant change in size distributions (153 nm vs 147 nm), surface charges (-14.8 mV vs -15.4 mV), nor concentrations of EVs (determined with NTA) before and after labelling.

3.2. CE-LIF of fluorescently labelled EVs

CE-LIF method development was first conducted with bovine milk-derived EVs isolated with sucrose gradient ultracentrifugation and suspended in phosphate-buffered saline (PBS) buffer. Keeping the EVs in PBS during CE separation represents the best-case scenario to maintain both physiological pH and isotonic conditions. This allowed us to focus on BGE optimization by reducing the risk of EVs loss or lysis induced from sample treatment steps. Several issues were however encountered during our preliminary tests using conventional BGEs for CE-LIF

(*i.e.* phosphate, borate, and Tricine/NaOH buffers). High conductivity of the PBS matrix of the samples was detrimental to CE stacking and separation, and adsorption of EVs to capillary wall led to undetectable and irreproducible signals. An effort was then made to exploit ‘inorganic-species-free’ (ISF) BGEs containing concentrated weakly charged molecules, which have recently been found to improve the performance of CE-LIF for proteins and peptides [28]. While both constituents of the ISF BGE used in this work are well known, the novelty lies in the use of unprecedentedly high concentrations (several hundred mM) of these large weakly charged molecules. Such high concentrations, while not favorable for conventional UV detection due to elevated background signal, were found advantageous for CE-LIF of EVs. This BGE at very high concentrations reduced spikes provoked by EVs aggregation / collision during electrophoresis, which was observed with other conventional BGEs. Interestingly, this observation was also reported in the recently released work on CE-UV of EVs, in which large ions (*i.e.* bis-tris propane ions) were employed to maintain the EV signal stability [18]. The ISF BGEs, which are tolerant to the presence of PBS in the sample matrix, were found to minimize protein adsorption to capillary wall and induce excellent stacking of slowly migrating proteins. They were expected to provide similar positive features when applied to EVs. The separations of labelled EVs from the abundant residual fluorophores in the PBS matrix are shown in Fig. 1. The ISF BGE was made up of Tris / CHES (pH 8.4) at different ionic strengths (50- 150 mM). The use of extremely high BGE concentrations (630 mM Tris and 870 mM CHES, IS: 150 mM) was still possible without generating high current intensity (only 30 μA under 25kV). Under the working conditions, the negatively charged EVs transported by an elevated EO mobility migrated faster than the residual CFDA-SE. The EO mobility was tuned from 26×10^{-9} to $12 \times 10^{-9} \text{ m}^2 \cdot \text{V}^{-1} \cdot \text{s}^{-1}$ by increasing IS from 50 to 150 mM. Under an IS of 90 mM (Fig. 1B), labelled EVs and CFSE fluorophore were much better separated than with IS of 50 mM (Fig. 1A), whereas the EV peak shape was not too broadened as was the case when observed with

IS of 150 mM (Fig. 1C). Sufficient resolution between EVs and CFSE fluorophore was needed to avoid peak overlapping due to a time-dependent increase in CFSE fluorophore peak. Indeed, CFSE-protein conjugates can exit EVs or become degraded over time [29]. Peaks of EVs were broad and many spikes appeared in the profile. To understand the origin of these events, the analysis was performed with a commercial PVA neutral coating, using the same BGE. As can be seen in Fig. 2, EVs peaks were still broad, this phenomenon being even more pronounced with the PVA coating that decreased the apparent EVs velocity. These results disproved the hypothesis that the broad peaks observed came from EVs adsorption to the silica capillary wall. The large peaks of EVs were most likely the result of a large size distribution of EVs (153 nm \pm 60 nm, obtained from three measurements of the same sample). It can also be observed from Figs. 1 and 2 that the longer the migration time of EVs is, the more the spikes on EVs' peaks can be visualized. The EV standards (bovine milk-derived EVs) used in this study had a high purity, thus excluding the possibility of impurity-induced spikes. Indeed, our results with LC-MS/MS (see Fig. S3 in ESI) showed that the major milk protein contaminants (e.g. α -s1 casein, α -s2 casein, β -casein and κ -casein) as well as some whey milk proteins such as α -Lactalbumin, serum albumin, etc.) were not detected in the EVs standards. Furthermore, the TEM pictures for bovine-milk derived EVs with negative staining by uranyl acetate proved again the high purity of EVs with the absence of the contaminant protein traces in the TEM images (Fig. S4 in ESI). The appearance of spikes during the CE of nanometric entities was already discussed in other studies on nanoparticles and was frequently related to the formation of aggregates [30, 31]. The particle aggregates can lead to some unwanted detector response (i.e. spike signals) due to the light scattering when passing through the detector [32, 33]. This common problem observed with nanoparticles was also observed during the CE of liposomes [34]. Interestingly, another recent work on CE-UV of EVs also revealed the presence of spikes during electrophoresis [18]. Since EVs suspended in PBS were injected to the CE-LIF, the presence of

PBS in the sample plugs (accounting for 10 % of the total capillary volume) are likely to produce local Joule heating under a high electrical field due to its high conductivity. The slower the migration of EVs in PBS under high voltages is, the longer EVs suffer from this local heating inside the capillary, which in turn provokes more spike-reflected aggregation. Due to the selectivity offered by LIF detection, only the peaks of EVs and those of fluorophore appeared in the electropherogram (see Fig. 1), allowing us to tolerate larger injection volumes. Our experimental data obtained with injection volumes from 2 % to 20 % of the total capillary volume (see Fig. S5 in ESI) revealed that an improvement of peak height was observed with an increase in injection volume, regardless of the tested sample matrix (i.e. PBS or 90 mM Tris/Ches). At large injection volumes of 15 and 20 %, the augmentation of peak intensity came with a penalty of peak distortion where the signal did not come back to the normal baseline after the EVs peak. Furthermore, the distance between the EVs peak and the fluorophore-induced plateau became much closer at injection volumes of 15-20 %, inducing more risk of peak overlapping upon inevitable increase in fluorescent signal over time (see section below). An injection volume of 10 % was found to be optimal, offering high signal intensity compared to that for the case of 2-3 % as in conventional hydrodynamic injection for CE, while maintaining sufficiently high separation resolution between EVs' and fluorophore's signals. Note also that, with the pioneering work on electrophoretic separation of EVs, we encountered more constraints than with the CE of nanoparticles (at least to our experience), notably more strict conditions for EVs stability, poorer signal intensity, and the high ionic-strength matrix required for biological entities which hinders efficient stacking. A compromise CE condition was therefore established taking into consideration all these constraints.

3.3. Matrix removal strategy

To avoid the aforementioned undesirable phenomenon during CE-LIF of EVs, two matrix cleanup approaches were tested, i) centrifugal filtration using Nanosep with Omega Membrane 3K, which was inspired from our previous work on matrix removal after fluorescent peptide labeling [35] and ii) EVs filtration with commercial Exosome Spin Columns (MW 3000) (see Fig. 3). In both cases, the EVs were recovered in the BGE. Both approaches offered efficient removal of redundant CSFA-SE, reflected by the absence of the peaks of fluorescent dyes. With the centrifugal filtration (Fig. 3B) multiple spikes were still detected. The aggregation of EVs was still induced in this case, presumably due to the centrifugal force at 5000 rpm required to eliminate the PBS ions through the 3K filter. However, such spikes were not observed when the sample was filtered with the Spin Column (Fig 3C). Furthermore, unsatisfactory EVs recovery (less than 60%) was obtained with the centrifugal filtration approach, compared to that achieved with the Spin Column-based alternative (75 % recovery, with deviation less than 5 % for a repeatability test on 4 EV samples), presumably due to EVs sticking to the NanoSep filter membranes [36]. A similar observation on low EVs recovery and reproducibility after filtration was also made in a recent work on CE-UV separation of EVs [18].

In a related context, another challenge encountered was to minimize or eliminate the lysis of EVs during analysis. Several studies have shown that EVs are stable under isotonic and hypotonic solutions [37, 38]. At the same time, if the IS (or conductivity) of the EVs sample matrix is higher than that of the BGE, this would lead to unfavorable de-stacking of EVs during CE-LIF with degraded peak shape and detection sensitivity. To find a compromise, matrix substitution after the Spin Column-based filtration was implemented with water and Tris / CHES having IS from 5 to 90 mM. The respective electropherograms using the optimized BGE are shown in Fig. 4. The best signal of EVs was achieved for the sample matrix composed of Tris / CHES IS 90 mM. The signal-to-noise ratios for EVs peaks dropped from 524 to 89 with

IS decreasing from 90 mM to 0 mM (DI water). Compared to other more diluted sample matrices, the 90 mM Tris / CHES did not produce any stacking effect since the matrix shares the same composition and concentration as the BGE employed. On the other hand, the rate of EVs lysis may be slowed down thanks to the IS being closer to isotonic conditions, resulting in a higher signal for EVs even without stacking effect. Sample matrices composed of Tris / CHES at higher IS (up to 240 mM) were also tested, but unsatisfactory data were obtained (data not shown) due to the unfavorable de-stacking with broader peaks when the IS of the sample matrix was higher than that of the BGE. The salient performance data obtained from these optimized conditions are shown in Table 1. The best detection limit for EVs achieved using the developed CE-LIF method reached approximately 8×10^9 EVs / mL whereas the calibration curve was acquired up to 1.20×10^{11} EVs / mL. The correlation between EVs concentrations and peak areas ($R^2 = 0.968$) was not optimal. It was nevertheless deemed satisfactory, taking into consideration that it comprises all the operational errors accumulated from the different steps, including EVs labeling, buffer substitution, electrokinetic separation and LIF detection. In the recent work on CE-UV of EVs [18], the linear correlation achieved was also far from optimal ($R^2 = 0.81$), confirming the challenges currently encountered with electrokinetic separation of EVs. Note that the working EVs volume of 40 μ L during the buffer substitution was at the lower limit of the recommended range (20-100 μ L) for Exosome Spin columns, which in turn may lead to some dilution errors. Larger working volumes were not available due to limited EVs concentrations and limited initial sample volumes. Better performance would nevertheless be expected when working with more concentrated EVs samples. To minimize fluorescent signal deviation due to sample degradation over time after buffer substitution (evidenced by reappearance of fluorophore signals in the electropherogram of Fig. S6), a calibration curve was made with four samples of different concentrations prepared in parallel and analyzed

promptly within the same day. Excellent intermediate precision was achieved for migration times (RSD < 0.6%) whereas a satisfactory one was obtained for peak areas (RSD < 5%).

3.4. Electrokinetic distribution of EVs from different animal and human origins

3.4.1. EVs purified with SEC or ultracentrifugation

Batches of EVs isolated from different animal and human origins using the established method (i.e. SEC and ultracentrifugation) were analyzed with our optimized CE-LIF method to demonstrate its potential in distinguishing EVs subpopulations based upon their electrophoretic mobilities (see Fig. 5). The EOF was measured before and after each EVs sample analysis and was shown to be remarkably stable (RSD less than 0.5 % over the whole analysis series). The difference in migration times observed between different EVs populations hence came purely from variation in their electrophoretic mobilities. The size distributions of the EVs isolates measured with NTA were also included in Fig. 5 for cross comparison with results obtained with CE-LIF. To interpret further the obtained results, our initial efforts to related migration behavior of EVs to their physicochemical characteristics (notably size, charge, charge/size ratio and shape) were made based on previous studies on CE of nanoparticles (NPs). Both EVs and NPs were thought to share similar size and charge characteristics. After this deep investigation we came to the conclusion that the dependency of NPs' electrophoretic mobilities on their size, charge, charge-to-size ratio and shape cannot be determined by a general rule, but was rather possible only for very specific situations and under some specific conditions [39-42]. Indeed, many parameters should be well considered and defined before a clear correlation between the electrophoretic mobilities of NPs and one of their particular characteristics can be established. Parameters such as BGE ionic strength, pH and composition, applied electrical field, injected amount of NPs etc. were found to have impacts on NPs' electrophoretic mobilities ([43] and other references listed therein). This makes it very difficult to rule out the dependency of NPs

electrophoretic mobilities on a single parameter. In the case of EVs, the situation is even more complicated, since their size distributions are broader and different sub-populations can co-exist (as reflected by NTA data). With bovine milk-derived EVs (Fig. 5A) one main peak was detected with CE-LIF and NTA, evidencing a low degree of polydispersity. A large size distribution of $175 \text{ nm} \pm 60 \text{ nm}$ was observed in this case according to NTA measurements. This observation is contrary to the case of CE of nanoparticles reported by Jones *et al.*, in which sharp peaks reflected different particle populations, but each having a narrow particle size distribution [44]. A low degree of polydispersity however was not the case with pony plasma-derived EVs (Fig. 5B) or serum-derived EVs (Fig. 5C) where two subpopulations were clearly identified with CE-LIF, and several size-based peaks were observed with NTA. An interesting observation was made on human plasma-derived EVs (Fig. 5D), where NTA data demonstrated a relatively homogeneous size distribution whereas two equivalent subpopulations were revealed with CE-LIF, implying some pronounced population heterogeneity from the human EVs source. While a conclusion on the reason behind the different profiles obtained with CE-LIF and NTA cannot be made at this stage of proof-of-concept for electrokinetic characterization of EVs, we assumed that this was due to different origins of EVs. EVs from different origins probably have different proteins / biomolecules on their surface and also different shapes that may influence their electrophoretic mobilities. Note also that EVs can exhibit shape variations in different BGE conditions, similar to the behavior of cells. Lysis of EVs can also occur, requiring a careful and restricted selection of BGE composition and ionic strength. The application of a high electrical field, as suggested by Jones *et al.* and d'Orlyé *et al.* for better NPs separations [40, 44], could not be utilized for EVs because it would provoke lysis. As a result, when applying these to the CE-LIF separations of EVs from different origins (Fig. 5), it was difficult to draw any conclusion. A deeper characterization study would therefore be needed to elucidate the EVs electrophoretic migration behavior, using EVs with a

lower degree of polydispersity and narrower size distribution. Such pure EVs nevertheless are not yet available with existing methods for EV purification.

3.4.2. EVs isolated with monolithic disks via immunoaffinity chromatography

Our CE-LIF approach was used to verify the presence of subpopulation of EVs isolated with our recent method based on functionalized monolithic disks. The reported isolation protocol using anti-human CD61 antibody [17] was herein extended using monolithic disk immobilized with monoclonal anti-human CD9 antibody. While monolithic disks immobilized with anti-CD61 antibody allow collection of platelet-derived EVs with sizes of 30-130 nm [17], those immobilized with anti-CD9 antibody were expected to capture more specifically a potential EV subtype historically claimed as “exosomes”, since CD9 is a tetraspanin that is thought to be enriched specifically in exosomes [45]. Note that according to the MISEV guidelines from ISEV, it is still not possible to propose a specific and universal marker of one or the other type of EVs. Distinct elutions from these two monolithic disks, using either ammonium hydroxide or sodium bicarbonate-carbonate as eluents are shown in Fig. 6. For comparison purpose, some NTA data for such elutions were provided in Fig. S7 in the ESI. From the electropherograms, three EV subpopulations from each of these elutions () were detected with CE-LIF. Three fractions were also detected with asymmetrical flow field-flow fractionation (AsFIFFF) in our previous work [17], proving the concordance of the results obtained with CE-LIF. Based on the CE-LIF signal intensity, the highest concentration was found for the fraction with longest migration time (17 min). . When monolithic disks immobilized with anti-CD9 antibody were employed, the signal of the second peak zone (10-12 min) became more intense (Fig. 6D). As already discussed in the session above, no conclusion on the precise size and charge of EV subpopulations visualized with CE-LIF could be made due to the lack of reference data for the fractions collected after the elution step. In an effort to give a deeper insight into EVs after the

monolithic affinity step, AsFIFFF was employed to further fractionate these eluents. Our CE-LIF approach was used to verify the quality of these EV fractions collected with AsFIFFF. .. Due to considerably lower EV concentrations in the AsFIFFF fractions compared to the whole monolithic disk isolates, lyophilization was used to enrich EVs prior to CE-LIF. This process was shown not to change the properties of EVs, or at least their physical characteristics [46]. The electropherograms for the AsFIFFF fractions expected to contain small EVs were shown in dashed lines in Figs. 6C and D. As can be seen, the presence of EVs in the AsFIFFF fractions (Fig. 6) was confirmed by the superposition of their profiles on those of the bulk collects.. Based on our results, the CE-LIF shows a real potential in distinguishing different EV subpopulations from highly specific EV isolates, which provides crucial information for future studies in the EV field. The developed CE-LIF method visualized the EVs distribution in AsFIFFF fractions and demonstrated that further optimization in the AsFIFFF method would be needed to obtain purer fractions of the EV subpopulations. Interestingly, higher LIF intensities were always observed on carbonate-bicarbonate elutions (Figs. 6 C, D) compared to those of ammonium hydroxide ones (Figs. A, B), regardless of the antibody used. This led us to a deeper study on CFDA-SE labelling in different media (see Fig. S6 in the ESI), which confirmed the less efficient labelling under an ammonium hydroxide medium due to unwanted conversion of CFDA-SE into side products in the presence of ammonium / amine groups.

4. Conclusion remarks

We successfully developed a fast and reliable CE-LIF method for the determination of labelled EVs, providing the first evidence that CE can be applied to distinguish EVs subpopulations from EV isolates, based on their electrophoretic mobilities. This new tool for the elucidation of electrokinetic distribution of EV populations adds valuable information to commonly-used size-based physical techniques such as NTA and transmission electron microscopy. The

applicability of the CE-LIF approach was successfully demonstrated for tracing of EVs from different origins, as well as for quality control of EVs after isolation with different methods including monolithic disks and subpopulation fractionation with AsFIFFF. Inclusion of a forefront isolation step from highly complex biofluids into an integrated microfluidic platform is now envisaged for the electrokinetic characterization of EV subpopulations with tiny sample volumes and low EV concentrations. Translation of batchwise EV sample treatment protocol into an integrated microfluidic platform is also desirable to reduce operation time and avoid cross contamination and EV loss. Prospective work to establish a solid theoretical background for the electrokinetic profiling of EVs will also be implemented when EVs with a better degree of polydispersity and narrower size (and charge) distribution could be obtained through improvement of EV purification technologies.

Acknowledgement

This work has been financially supported by the Institut Universitaire de France (for M. Taverna, senior member). The doctoral scholarship for Marco Morani was supported by the doctoral school 2MIB (Sciences Chimiques: Molécules, Matériaux, Instrumentation et Biosystèmes) – University Paris Saclay. We thank Ms. Oihana Inda-Arsa for preliminary explorations in CE-UV and CE-LIF. Dr. Hervé Hillaireau and Magali Noiray from Institute Galien Paris Sud – University Paris Saclay are acknowledged for their help and support in NTA measurements. We thank Mr. Edward Mitchell for English grammar corrections. Financial support (E.M. and M.-L.R.) was also provided by the Research Council for Natural Sciences and Engineering, Academy of Finland (grant No 1311369)

The authors have declared no conflict of interest.

References:

- [1] G. van Niel, G. D'Angelo, G. Raposo, Shedding light on the cell biology of extracellular vesicles, *Nat. Rev. Mol. Cell Biol* 19 (2018) 213-228.
- [2] G. Raposo, W. Stoorvogel, Extracellular vesicles: Exosomes, microvesicles, and friends, *J. Cell Biol.*, 200 (2013) 373-383.
- [3] H.C. Bu, D.G. He, X.X. He, K.M. Wang, Exosomes: Isolation, Analysis, and Applications in Cancer Detection and Therapy, *ChemBiochem*, 20 (2019) 451-461.
- [4] M.T. Guo, A. Rotem, J.A. Heyman, D.A. Weitz, Droplet microfluidics for high-throughput biological assays, *Lab on a Chip*, 12 (2012) 2146-2155.
- [5] J. Howitt, A.F. Hill, Exosomes in the Pathology of Neurodegenerative Diseases, *Journal of Biological Chemistry*, 291 (2016) 26589-26597.
- [6] H.L. Shao, H. Im, C.M. Castro, X. Breakefield, R. Weissleder, H.H. Lee, New Technologies for Analysis of Extracellular Vesicles, *Chemical Reviews*, 118 (2018) 1917-1950.
- [7] E.H. Koritzinsky, J.M. Street, R.A. Star, P.S.T. Yuen, Quantification of Exosomes, *J. Cell. Physiol.*, 232 (2017) 1587-1590.
- [8] R. Szataneck, M. Baj-Krzyworzeka, J. Zimoch, M. Lekka, M. Siedlar, J. Baran, The Methods of Choice for Extracellular Vesicles (EVs) Characterization, *Int. J. Mol. Sci.*, 18 (2017).

- [9] U. Erdbrugger, J. Lannigan, Analytical Challenges of Extracellular Vesicle Detection: A Comparison of Different Techniques, *Cytometry Part A*, 89A (2016) 123-134.
- [10] S. Biosciences, FluoroCet exosome quantitation kit https://www.systembio.com/wp-content/uploads/MANUAL_FCET96A-1-1.pdf, (2017).
- [11] T. Hikita, M. Miyata, R. Watanabe, C. Oneyama, Sensitive and rapid quantification of exosomes by fusing luciferase to exosome marker proteins, *Sci. Reports*, 8 (2018).
- [12] M. Al Ahmad, Electrical Detection, Identification, and Quantification of Exosomes, *Ieee Access*, 6 (2018) 22817-22826.
- [13] L. Trapiella-Alfonso, G. Ramirez-Garcia, F. d'Orlye, A. Varenne, Electromigration separation methodologies for the characterization of nanoparticles and the evaluation of their behaviour in biological systems, *Trac-Trends Anal. Chem.*, 84 (2016) 121-130.
- [14] T. Akagi, K. Kato, M. Kobayashi, N. Kosaka, T. Ochiya, T. Ichiki, On-Chip Immunoelectrophoresis of Extracellular Vesicles Released from Human Breast Cancer Cells, *Plos One*, 10 (2015).
- [15] K. Kato, M. Kobayashi, N. Hanamura, T. Akagi, N. Kosaka, T. Ochiya, T. Ichiki, Electrokinetic Evaluation of Individual Exosomes by On-Chip Microcapillary Electrophoresis with Laser Dark-Field Microscopy, *Jpn. J. Appl. Phys.*, 52 (2013).
- [16] T. Akagi, K. Kato, N. Hanamura, M. Kobayashi, T. Ichiki, Evaluation of desialylation effect on zeta potential of extracellular vesicles secreted from human prostate cancer cells by on-chip microcapillary electrophoresis, *Jpn. J. Appl. Phys.*, 53 (2014).
- [17] E. Multia, C.J.Y. Tear, M. Palviainen, P. Siljander, M.-L. Riekkola, Fast isolation of highly specific population of platelet-derived extracellular vesicles from blood plasma by affinity monolithic column, immobilized with anti-human CD61 antibody, *Anal. Chim. Acta*, 1091 (2019) 160-168.

- [18] M. Piotrowska, K. Ciura, M. Zalewska, M. Dawid, B. Correia, P. Sawicka, B. Lewczuk, J. Kasprzyk, L. Sola, W. Piekoszewski, B. Wielgomas, K. Waleron, S. Dziomba, Capillary zone electrophoresis of bacterial extracellular vesicles: A proof of concept, *J. Chromatogr. A*, (2020) 461047.
- [19] O.H. Lowry, N.J. Rosebrough, A.L. Farr, R.J. Randall, Protein measurement with the folin phenol reagent, *J. Biol. Chem.*, 193 (1951) 265-275.
- [20] M. Puhka, M.E. Nordberg, S. Valkonen, A. Rannikko, O. Kallioniemi, P. Siljander, T.M. af Hallstrom, KeepEX, a simple dilution protocol for improving extracellular vesicle yields from urine, *Eur. J. Pharm. Sci*, 98 (2017) 30-39.
- [21] A. Hellqvist, Y. Hedeland, C. Pettersson, Evaluation of electroosmotic markers in aqueous and nonaqueous capillary electrophoresis, *Electrophoresis*, 34 (2013) 3252-3259.
- [22] A. Hoshino, B. Costa-Silva, T.L. Shen, G. Rodrigues, A. Hashimoto, M.T. Mark, H. Molina, S. Kohsaka, A. Di Giannatale, S. Ceder, S. Singh, C. Williams, N. Soplol, K. Uryu, L. Pharmed, T. King, L. Bojmar, A.E. Davies, Y. Ararso, T. Zhang, H. Zhang, J. Hernandez, J.M. Weiss, V.D. Dumont-Cole, K. Kramer, L.H. Wexler, A. Narendran, G.K. Schwartz, J.H. Healey, P. Sandstrom, K.J. Labori, E.H. Kure, P.M. Grandgenett, M.A. Hollingsworth, M. de Sousa, S. Kaur, M. Jain, K. Mallya, S.K. Batra, W.R. Jarnagin, M.S. Brady, O. Fodstad, V. Muller, K. Pantel, A.J. Minn, M.J. Bissell, B.A. Garcia, Y. Kang, V.K. Rajasekhar, C.M. Ghajar, I. Matei, H. Peinado, J. Bromberg, D. Lyden, Tumour exosome integrins determine organotropic metastasis, *Nature*, 527 (2015) 329-+.
- [23] H.D. Roberts-Dalton, A. Cocks, J.M. Falcon-Perez, E.J. Sayers, J.P. Webber, P. Watson, A. Clayton, A.T. Jones, Fluorescence labelling of extracellular vesicles using a novel thiol-based strategy for quantitative analysis of cellular delivery and intracellular traffic, *Nanoscale*, 9 (2017) 13693-13706.

- [24] J. Lannigan, U. Erdbruegger, Imaging flow cytometry for the characterization of extracellular vesicles, *Methods*, 112 (2017) 55-67.
- [25] A. Morales-Kastresana, B. Telford, T.A. Musich, K. McKinnon, C. Clayborne, Z. Braig, A. Rosner, T. Demberg, D.C. Watson, T.S. Karpova, G.J. Freeman, R.H. DeKruyff, G.N. Pavlakis, M. Terabe, M. Robert-Guroff, J.A. Berzofsky, J.C. Jones, Labeling Extracellular Vesicles for Nanoscale Flow Cytometry, *Sci. Rep.*, 7 (2017).
- [26] M. Dehghani, S.M. Gulvin, J. Flax, T.R. Gaborski, Exosome labeling by lipophilic dye PKH26 results in significant increase in vesicle size, *bioRxiv*, (2019) 532028.
- [27] X.Q. Wang, X.M. Duan, L.H. Liu, Y.Q. Fang, Y. Tan, Carboxyfluorescein diacetate succinimidyl ester fluorescent dye for cell Labeling, *Acta Biochim. Biophys. Sin.*, 37 (2005) 379-385.
- [28] M. Morani, M. Taverna, T.D. Mai, A fresh look into background electrolyte selection for capillary electrophoresis-laser induced fluorescence of peptides and proteins, *Electrophoresis*, 40 (2019) 2618-2624.
- [29] H.T. Banks, A. Choi, T. Huffman, J. Nardini, L. Poag, W.C. Thompson, Quantifying CFSE label decay in flow cytometry data, *Appl. Math. Lett.*, 26 (2013) 571-577.
- [30] C. Quang, S.L. Petersen, G.R. Ducatte, N.E. Ballou, Characterization and separation of inorganic fine particles by capillary electrophoresis with an indifferent electrolyte system, *Journal of Chromatography A*, 732 (1996) 377-384.
- [31] S.L. Petersen, N.E. Ballou, Separation of micrometer-size oxide particles by capillary zone electrophoresis, *Journal of Chromatography A*, 834 (1999) 445-452.
- [32] S. Dziomba, K. Ciura, B. Correia, B. Wielgomas, Stabilization and isotachopheresis of unmodified gold nanoparticles in capillary electrophoresis, *Analytica Chimica Acta*, 1047 (2019) 248-256.

- [33] S. Dziomba, K. Ciura, P. Kocialkowska, A. Prah, B. Wielgomas, Gold nanoparticles dispersion stability under dynamic coating conditions in capillary zone electrophoresis, *Journal of Chromatography A*, 1550 (2018) 63-67.
- [34] M.A. Roberts, L. LocascioBrown, W.A. MacCrehan, R.A. Durst, Liposome behavior in capillary electrophoresis, *Analytical Chemistry*, 68 (1996) 3434-3440.
- [35] C.C. de Lassichere, T.D. Mai, M. Otto, M. Taverna, Online Preconcentration in Capillaries by Multiple Large-Volume Sample Stacking: An Alternative to Immunoassays for Quantification of Amyloid Beta Peptides Biomarkers in Cerebrospinal Fluid, *Anal. Chem.*, 90 (2018) 2555-2563.
- [36] K.E. Petersen, F. Shiri, T. White, G.T. Bardi, H. Sant, B.K. Gale, J.L. Hood, Exosome Isolation: Cyclical Electrical Field Flow Fractionation in Low-Ionic-Strength Fluids, *Analytical Chemistry*, 90 (2018) 12783-12790.
- [37] E. Willms, H.J. Johansson, I. Mager, Y. Lee, K.E.M. Blomberg, M. Sadik, A. Alaarg, C.I.E. Smith, J. Lehtio, S.E.L. Andaloussi, M.J.A. Wood, P. Vader, Cells release subpopulations of exosomes with distinct molecular and biological properties, *Sci. Rep.*, 6 (2016) 12.
- [38] V.S. Chernyshev, R. Rachamadugu, Y.H. Tseng, D.M. Belnap, Y.L. Jia, K.J. Branch, A.E. Butterfield, L.F. Pease, P.S. Bernard, M. Skliar, Size and shape characterization of hydrated and desiccated exosomes, *Anal. Bioanal. Chem.*, 407 (2015) 3285-3301.
- [39] F. d'Orlye, A. Varenne, P. Gareil, Size-based characterization of nanometric cationic maghemite particles using capillary zone electrophoresis, *Electrophoresis*, 29 (2008) 3768-3778.
- [40] F. d'Orlye, A. Varenne, T. Georgelin, J.M. Siaugue, B. Teste, S. Descroix, P. Gareil, Charge-based characterization of nanometric cationic bifunctional maghemite/silica

- core/shell particles by capillary zone electrophoresis, *Electrophoresis*, 30 (2009) 2572-2582.
- [41] F.K. Liu, F.H. Ko, P.W. Huang, C.H. Wu, T.C. Chu, Studying the size/shape separation and optical properties of silver nanoparticles by capillary electrophoresis, *J. Chromatogr. A*, 1062 (2005) 139-145.
- [42] N.G. Vanifatova, B.Y. Spivakov, J. Mattusch, U. Franck, R. Wennrich, Investigation of iron oxide nanoparticles by capillary zone electrophoresis, *Talanta*, 66 (2005) 605-610.
- [43] U. Pyell, Characterization of nanoparticles by capillary electromigration separation techniques, *Electrophoresis*, 31 (2010) 814-831.
- [44] H.K. Jones, N.E. Ballou, Separations of chemically different particles by capillary electrophoresis, *Anal. Chem.*, 62 (1990) 2484-2490.
- [45] J. Kowal, G. Arras, M. Colombo, M. Jouve, J.P. Morath, B. Primdal-Bengtson, F. Dingli, D. Loew, M. Tkach, C. Théry, Proteomic comparison defines novel markers to characterize heterogeneous populations of extracellular vesicle subtypes, *PNAS*, 113 (2016) E968.
- [46] A.E. Russell, A. Sneider, K.W. Witwer, P. Bergese, S.N. Bhattacharyya, A. Cocks, E. Cocucci, U. Erdbrügger, J.M. Falcon-Perez, D.W. Freeman, T.M. Gallagher, S. Hu, Y. Huang, S.M. Jay, S.-i. Kano, G. Lavieu, A. Leszczynska, A.M. Llorente, Q. Lu, V. Mahairaki, D.C. Muth, N. Noren Hooten, M. Ostrowski, I. Prada, S. Sahoo, T.H. Schøyen, L. Sheng, D. Tesch, G. Van Niel, R.E. Vandenbroucke, F.J. Verweij, A.V. Villar, M. Wauben, A.M. Wehman, H. Yin, D.R.F. Carter, P. Vader, Biological membranes in EV biogenesis, stability, uptake, and cargo transfer: an ISEV position paper arising from the ISEV membranes and EVs workshop, *J. Extracell. Vesicles*, 8 (2019) 1684862.

Table 1: Calibration range, coefficient of determination (R^2) for linearity, limit of detection (LOD) and repeatability ($n = 3$) for the CE-LIF determination of fluorescently labelled EVs

Calibration range (EVs / mL) ^a	R^2	LOD (EVs / mL) ^b	RSD (%) migration times	RSD (%) peak areas
$1.22 \times 10^{10} - 12 \times 10^{10}$	0,968	7.86×10^9	0.6	4.3

^a 4 concentrations.

^b Based on peak heights corresponding to $S/N = 3$

Figure captions:

Fig. 1. CE-LIF of EVs (in PBS) derivatized with CFDA-SE, using ISF BGE Tris / CHES (pH 8.4) at different ionic strengths: A) 50 mM; B) 90 mM and C) 150 mM. Other CE conditions: uncoated fused silica capillary with I.D. of 50 μ m, effective length (l_{eff}) of 50.2 cm and total length (L_{tot}) of 60.2 cm; Applied voltage: +25 kV; hydrodynamic injection at 3.4 kPa for 2 min. LIF detection with $\lambda_{\text{ex}} = 488$ nm, λ_{em} : 520 nm.

Fig. 2. CE-LIF of EVs (in PBS) derivatized with CFDA-SE in PVA coated capillary A) I.D. of 50 μ m, effective length (l_{eff}) of 10 cm and total length (L_{tot}) of 60.2 cm using ISF BGE composed of Tris / CHES (IS 50 mM, pH 8.4); B) and C) I.D. of 50 μ m, effective length (l_{eff}) of 50.2 cm and total length (L_{tot}) of 60.2 cm using ISF BGE composed of Tris / CHES IS 50 mM and 90 mM (pH 8.4) respectively. Other CE conditions: -25 kV; $\lambda_{\text{ex}} = 488$ nm, λ_{em} : 520 nm.

Fig. 3. CE-LIF of fluorescently labeled EVs (A) without filtration (in PBS); (B) after matrix removal with Nanosep unit using a Omega 3K membrane and reconstitution in Tris / CHES (IS 90 mM, pH 8.4); and (C) with Exosome Spin Columns (MW 3000) and reconstitution in Tris / CHES 90 mM at pH 8.4. BGE: Tris / CHES (IS 90 mM, pH 8.4). Other CE conditions as described in Fig. 1.

Fig. 4. CE-LIF of fluorescently labeled EVs after matrix substitution with Exosome Spin Column (MW 3000) by Tris / CHES (pH 8.4) at different ionic strengths: A) 90 mM; B) 50 mM; C) 20 mM; D) 5 mM and E) DI water. Other CE conditions as described in Fig. 3.

Fig. 5. CE-LIF electropherograms *vs.* NTA profiles for fluorescently labeled EVs (after matrix removal with Exosome Spin Columns (MW 3000) and reconstitution in Tris / CHES 90 mM at pH 8.4). The EVs were purified from A) bovine milk; B) pony plasma; C) pony serum and D) human plasma. BGE: Tris / CHES (IS 90 mM, pH 8.4). Other CE conditions as described in Fig. 1.

Fig. 6 CE-LIF of fluorescently labeled EVs isolated with affinity monolithic disks (continuous lines) after matrix substitution into Tris / CHES 90 mM (pH 8.4) with Exosome Spin Columns (MW 3000). The dashed lines represent the EV < 50 nm fractions further purified with AsFIFFF after the elution step. EVs elution from monolithic disks under alkaline conditions (pH 11.3) was performed with: (A) (B) ammonium hydroxide; (C) (D) sodium bicarbonate-carbonate. Monolithic disks were immobilized with: (A)(C) anti-human CD61; (B)(D) anti-human CD9. Other CE conditions as described in Fig. 1

Figures:

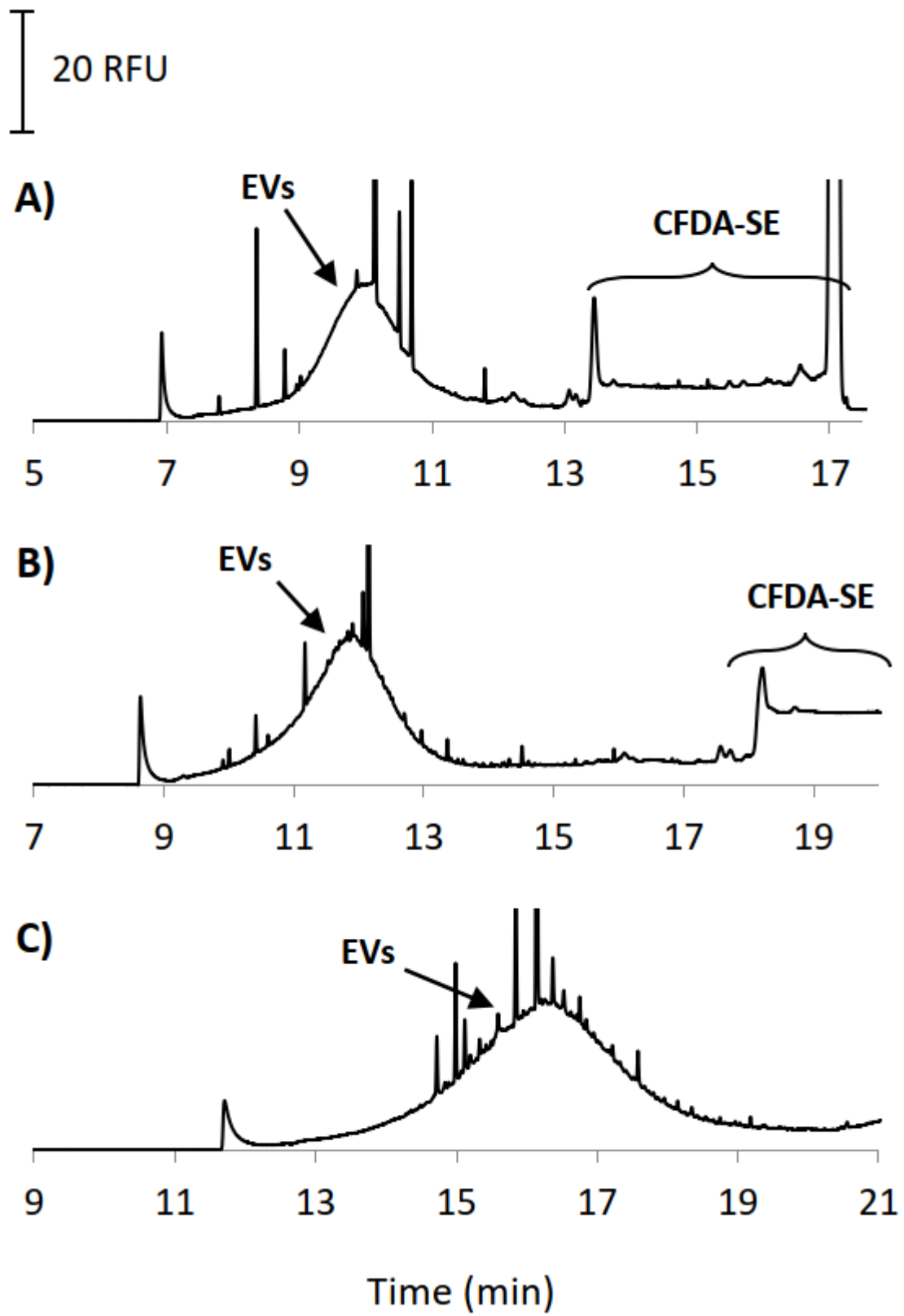


Fig. 1.

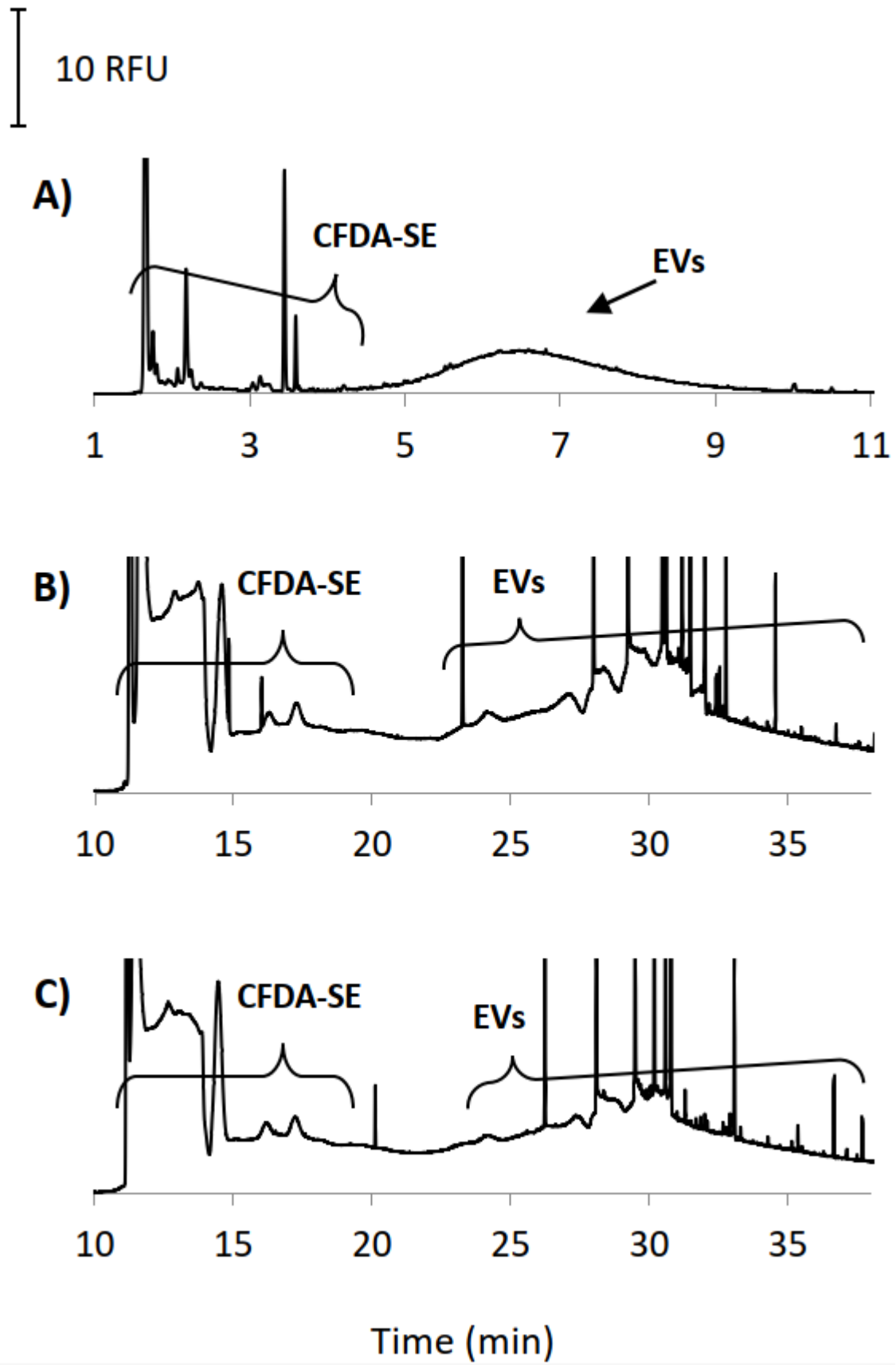


Fig. 2.

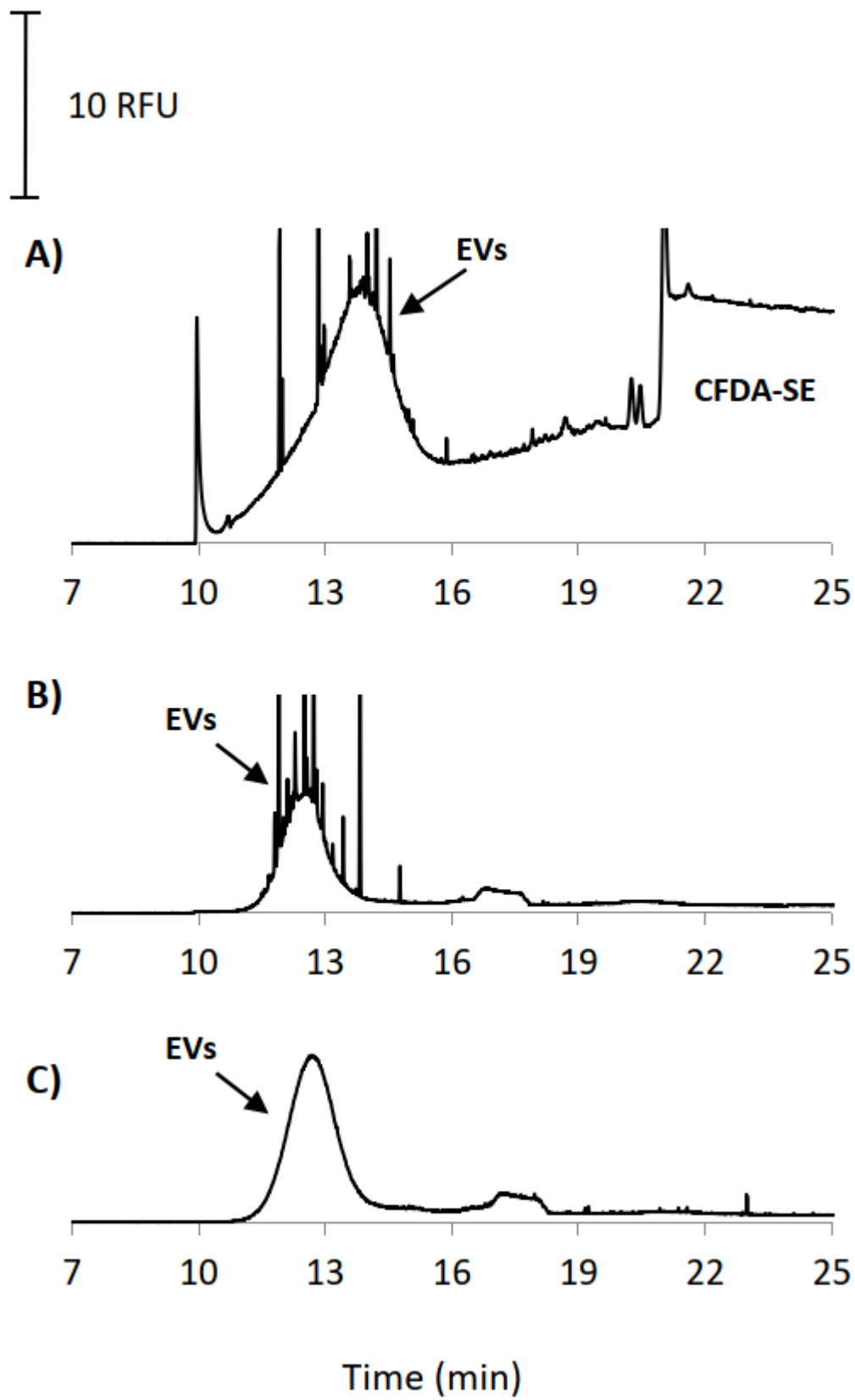


Fig. 3.

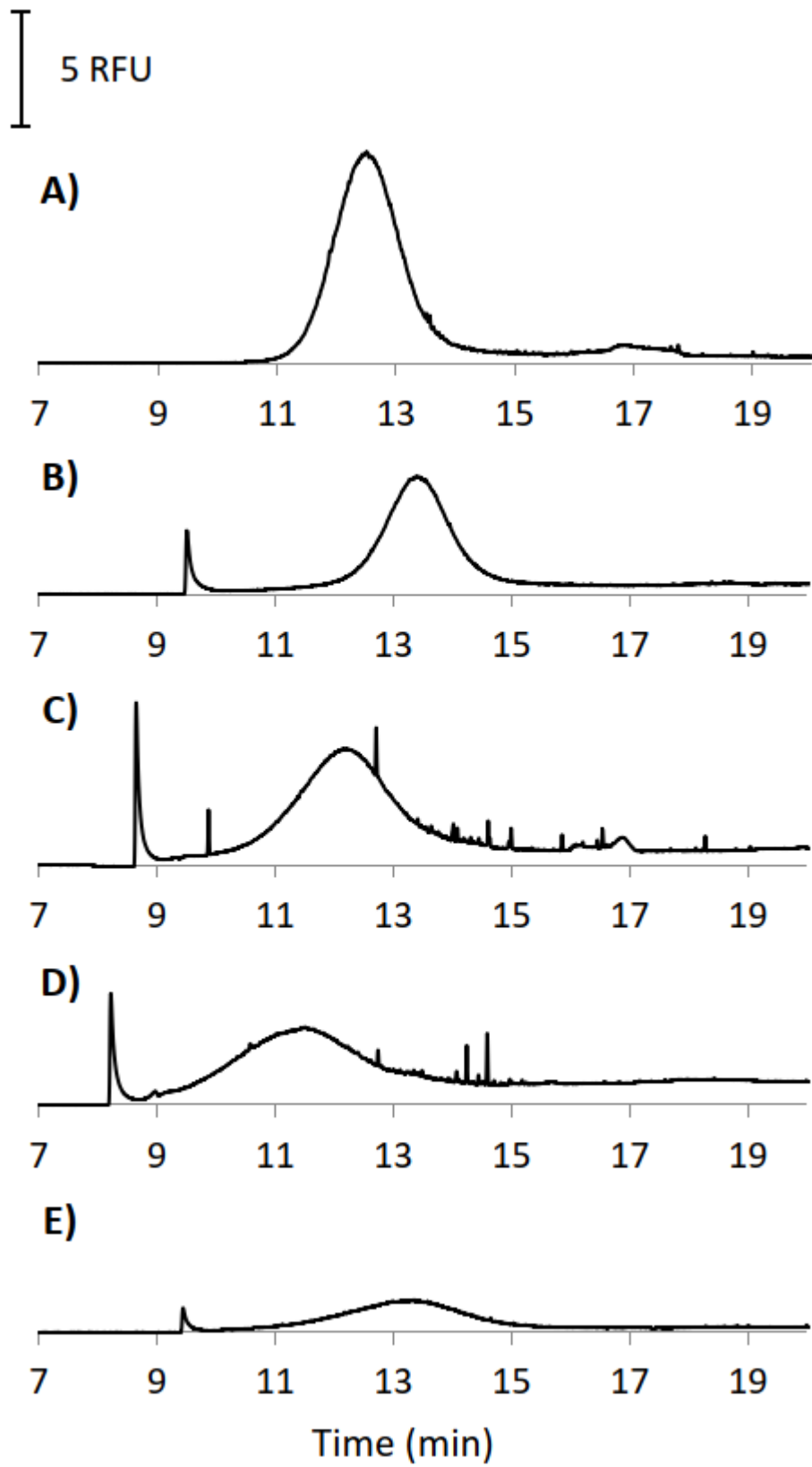


Fig. 4.

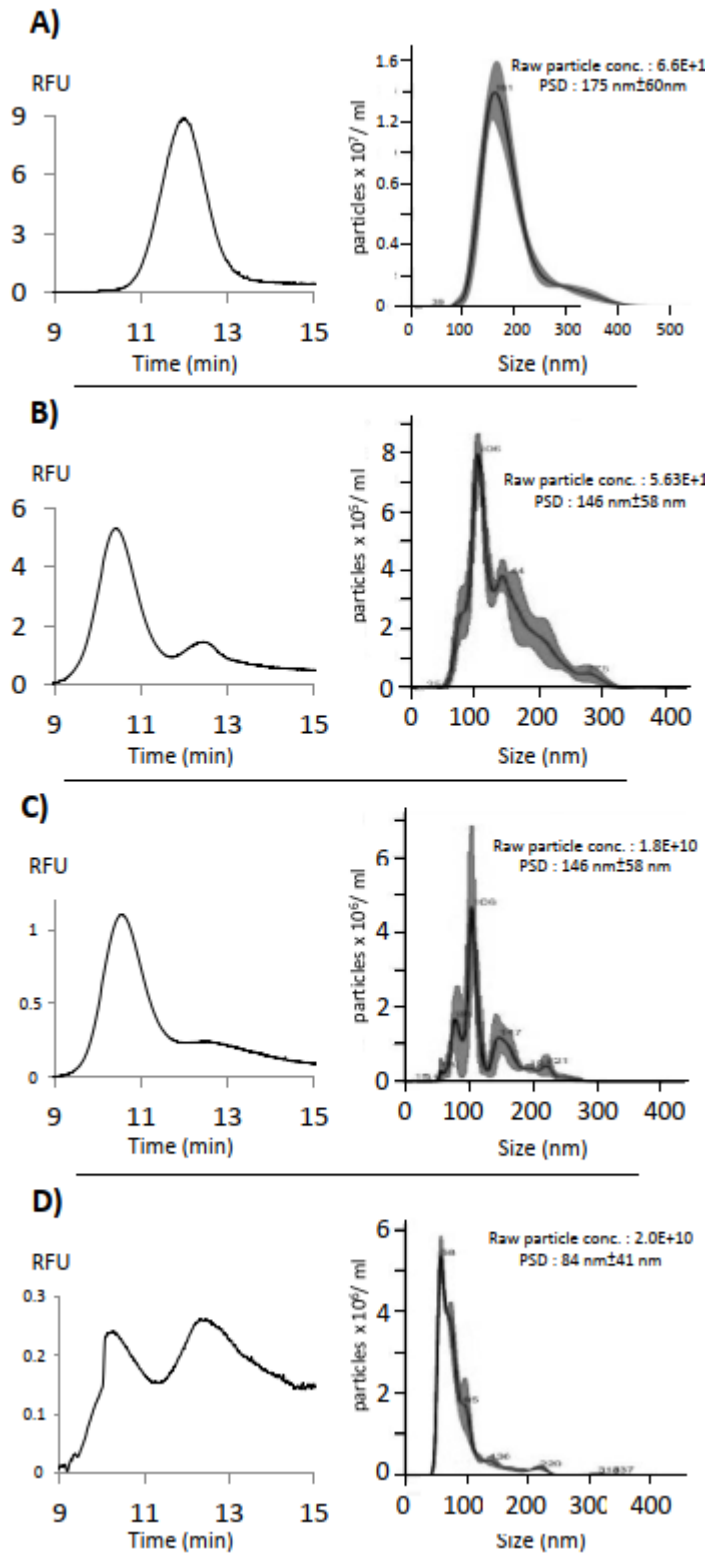


Fig. 5.

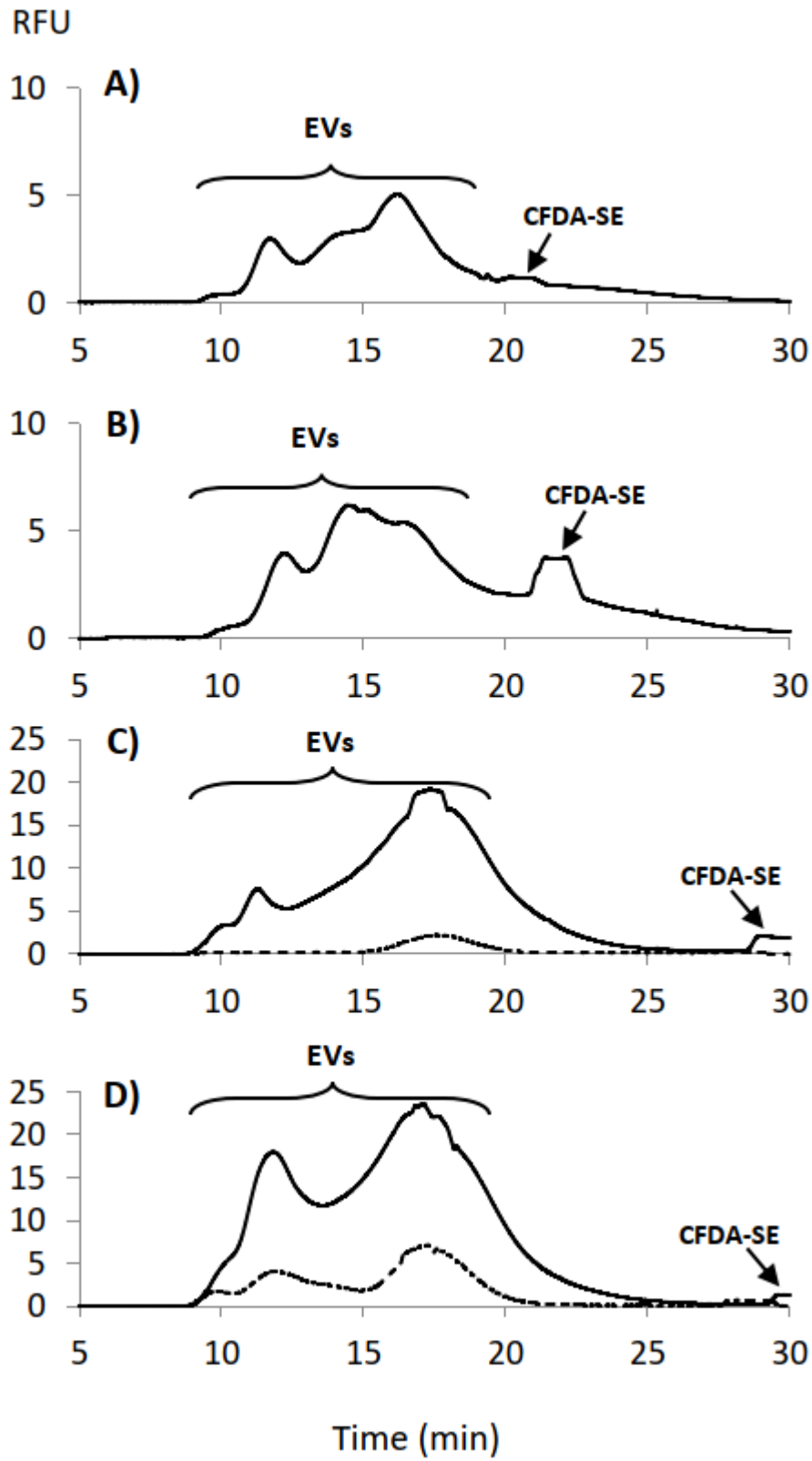


Fig. 6.